Universiteit
Antwerpen

This item is the archived peer-reviewed author-version of:

Effect of electric field and vertical strain on the electro-optical properties of the MoSi2N4 bilayer : a first-principles calculation

Reference:
Bafekry Asadollah, Stampfl C., Naseri M., Fadlallah Mohamed M., Faraji M., Ghergherehchi M., Gogova D., Feghhi S.A.H..- Effect of electric field and vertical strain on the electro-optical properties of the MoSi2N4 bilayer : a first-principles calculation
Journal of applied physics / American Institute of Physics - ISSN 0021-8979 - 129:15(2021), 155103
Full text (Publisher's DOI): https://doi.org/10.1063/5.0044976
To cite this reference: https://hdl.handle.net/10067/1782330151162165141

uantwerpen.be
Institutional repository IRUA

Effect of electric field and vertical strain on the electro-optical properties of the $MoSi_2N_4$ bilayer: A First-Principles calculation

A. Bafekry,[1,2,*] C. Stampfl,[3] M. Naseri,[4] M. M. Fadlallah,[5] M. Faraji,[6] M. Ghergherehchi,[7] D. Gogova,[8] and S. A. H. Feghhi[1]

[1]*Department of Radiation Application, Shahid Beheshti University, Tehran 1983969411, Iran*
[2]*Department of Physics, University of Antwerp, Groenenborgerlaan 171, B-2020 Antwerp, Belgium*
[3]*School of Physics, The University of Sydney, NSW 2006, Australia*
[4]*Department of Physics, Kermanshah Branch, Islamic Azad University, 6718997551, Kermanshah, Iran*
[5]*Department of Physics, Faculty of Science, Benha University, 13518 Benha, Egypt*
[6]*Micro and Nanotechnology Graduate Program, TOBB University of Economics and Technology, Sogutozu Caddesi No 43 Sogutozu, 06560, Ankara, Turkey*
[7]*College of Electronic and Electrical Engineering, Sungkyunkwan University, Suwon, Korea*
[8]*Department of Physics, University of Oslo, P.O. Box 1048, Blindern, Oslo, Norway*

Recently a two-dimensional (2D) $MoSi_2N_4$ (MSN) structure has been successfully synthesized [Hong et al., Sci. 369, 670 (2020)]. Motivated by this result, we investigate the structural, electronic and optical properties of MSN monolayer (MSN-1L) and bilayer (MSN-2L) under the applied electric field (E-field) and strain using density functional theory calculations. We find that the MSN-2L is a semiconductor with an indirect band gap of 1.60 (1.80) eV using PBE (HSE06). The band gap of MSN-2L decreases as the E-field increases from 0.1 to 0.6 V/Åand for larger E-field up to 1.0 V/Å the bilayer becomes metallic. As the vertical strain increases the band gap decreases; more interestingly, a semiconductor to a metal phase transition is observed at a strain of 12%. Furthermore, the optical response of the MSN-2L is in the ultraviolet (UV) region of the electromagnetic spectrum. The absorption edge exhibits a blue shift by applying an E-field or a vertical compressive strain. The obtained interesting properties suggest MSN-2L as a promising material in electro-mechanical and UV opto-mechanical devices.

I. INTRODUCTION

Recently, two-dimensional (2D) materials have been found to exhibit unique structural, electronic, and optical properties, due to their high surface to volume ratio, low phonon energy, high ionicity and tunability.[1] These outstanding properties have made them one of the most intriguing family of materials for potential applications in nanoelectronic and optoelectronic devices including, field-effect transistors,[2] Li-ion batteries,[3] supercapacitors,[4] solar cells,[5] photodetectors,[6] lasers,[7] light-emitting diodes[8] and so on. Several 2D nanosheets including, graphene,[9] Mxenes,[10–12] transition metal dichalcogenides (TMDCs)[13] and boron nitride (BN),[14] have been extensively studied both experimentally and theoretically.

Among the aforementioned 2D structures, Mxenes are of high current interest due to potential technological applications. The general formula of Mxenes is $M_{n+1}X_nT_x$ (where M refers to transition metals such as Ti, Cr, Mo; X can be N and C; and finally, T is related to surface termination by halogens, chalcogenide elements, and other groups such as OH). The unique combination of properties of Mxenes nanosheets arises from two participating transition metals in the structure. Mxenes possess high mechanical stability and electrical conductivity, a negative zeta-potential, and efficient electromagnetic waves adsorption, which has led to a strong scientific interest with regard to potential applications. The nanosheets can be modified using several processes including application of electric field (E-field), adatom chemisorption, doping with different impurity elements, and application of biaxial and uniaxial strain.[15–31] The optical and electronic properties of semiconductors can be tailored for example by conversion of an indirect band gap to a direct one and changing its value. In addition, an insulating nanosheet can be converted to a semiconductor or a metal, and magnetism can be introduced into a nonmagnetic structure. One of the modification approaches, the application of an E-field is quite desirable because of its unique ability to change optical and electrical properties by variation of the Fermi-level and electronic states of the structure.

Y. Lan *et al.*[32] studied the band structure of the van der Waals graphene/$MoTe_2$ heterostructure for biaxial strain and different E-fields by means of first-principles calculations. After heterostructure formation, the Fermi level shifted to the conduction band minimum (CBM) of the $MoTe_2$ layer, becoming an n-type Schottky contact. The type, and Schottky barrier height (SBH), of contact at the interface could be modified by applying an external field or by strain. The E-field has adjusted the heterostructure to the Ohmic contact at both negative and positive sides. On application of biaxial strain, when the compressive and tensile strain reached 10 and 7%, respectively, an Ohmic contact also emerged. Consequently, it was demonstrated that applying strain or an E-field is one of the best ways to control the type of contact, as well as varying the SBH of the heterostructure. To design high-performance optoelectronic and nanoelectronic devices, these features are considered important. M. Luo and H. Yin[33] systematically investigated the op-

tical and electronic properties of δ-SnSe, β-SnSe, and α-SnSe monolayers under application of an E-field by means of first-principles calculations. The E-field was found to reduce the band gap of the δ-SnSe nanosheet from 2.23 to 1.26 eV. This change was due to the p states of the Se and Sn atoms. Additionally, they calculated the dielectric properties of the three nanosheets under the E-field, and for the α-SnSe monolayer, it was found that the light absorption properties in the range of infrared and visible light were significantly promoted.

In Ref. 34, we study theoretically the structural, mechanical, thermal, electronic and optical properties of the $MoSi_2N_4$ monolayer employing DFT calculations. Here, the focus is on the modification of the $MoSi_2N_4$ mono and bi-layer electro-optical properties by an external electrical field and mechanical strain. To the best of our knowledge such a study does not exist in the literature.

II. METHOD

Here, for the aim of electronic and optical properties assessing, full-potential linearized augmented plane-wave method (FLAPW) based on the density functional theory (DFT) as implemented in WIEN2K[37] was employed. As the first step, atomic coordinates optimization was done by using generalized gradient approximation (GGA) in the form of Perdew-Burke-Ernzerhof (PBE).[38,39] For the electronic properties, the first Brillouin zone (BZ) was sampled by $12 \times 12 \times 1$ k-points for one unit cell. The input parameters of $R_{MT}\ K_{max}$ =7, G_{max}=14 Ry$^{1/2}$ and l_{max} =10 were considered. A denser k-point mesh of $22 \times 22 \times 1$ was utilized for the optical properties calculations.[41] To avoid possible interlayer interaction, an empty space of 20 Å was used along the none periodic direction. The Bader charge analysis[40] was utilized to determine the electron charge transfer, and the vibrational properties were computed by the finite-displacement method implemented in the PHONOPY code.[42] For more detail about calculations of optical properties see supporting information (SI).

III. MONOLAYER

The top and side views of the atomic structure of MSN-1L are illustrated in Fig. 1(a). From the top view, the MSN-1L, Mo, Si, and N atoms are packed in a honeycomb lattice, forming a 2D crystal with a space group of P_{6m1}. The hexagonal primitive unit cell (indicated by red parallelogram) is formed by 7 atoms (involving 1 Mo, 2 Si and 4 N atoms). After structure optimization the calculated lattice constant is 2.91 Å, while the bond lengths of Mo-N and Si-N are 1.75 and 1.74 Å, respectively. The two angles of Si-N-Si are determined as 112° and 106°, while the two angles of Si-Mo-Si are 87° and 73°. The thickness (t) of MSN-1L is 7.01 Å. These results agree well with a previous report.[35]

The cohesive energy (E_{coh}), which is defined as the energy gained on bringing free, isolated atoms together to form the structure, is one of the most important physical parameters in quantifying the energetic stability of materials. The cohesive energy per atom is calculated as:

$$E_{coh} = \frac{E_{Mo} + 2E_{Si} + 4E_N - E_{tot}}{n_{tot}}, \qquad (1)$$

where E_{Mo}, E_{Si} and E_N, E_{tot} represent the energies of isolated Mo, Si, N atoms and total of the monolayer, and n_{tot} is the total number of atoms, respectively. The calculated energy is -8.46 eV/atom. The negative sign indicates that the structure is exothermic. The dynamical stability of MSN-1L is verified by calculating the phonon dispersion curves, which are presented in Fig. 1(b). It can be seen that there are no imaginary frequencies indicating the dynamical stability of the structure. The contour plot of the electron localization function (ELF) is shown in Fig. 1(c), where red (blue) color indicates high (low) electron density. The negatively charged N atoms are surrounded by positively charged Si and Mo atoms due to a transfered charge from Si and Mo atoms to N atom. The Badar charge analysis reveals that each N atom gains 1.5 and 2.23 e from the neighboring Mo and Si atoms, respectively.

The calculated electronic band structures, density of

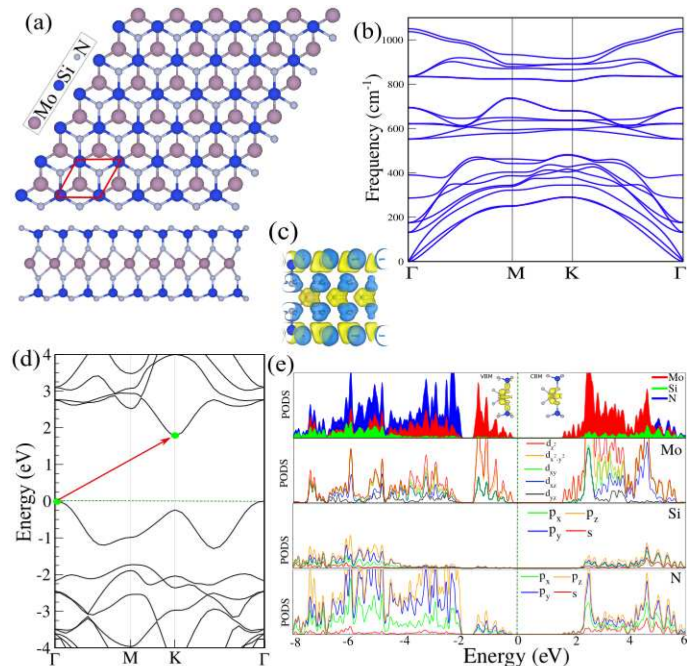

Figure 1. (a) Atomic structure, (b) phonon band dispersion, (c) isosurface plot of the electron localization function (ELF), (d) electronic band structure and (e) DOS and PDOS of MSN-1L. The primitive unit cell is indicated by a red parallelogram. The spatial electron densities of the valance band maximum (VBM) and conduction band minimum (CBM) states are shown in the inset of the DOS. The zero of energy is set to the Fermi-level.

Table I. The structural and electronic parameters including lattice constant a,b; Si-N and Mo-N bond lengths; Si-N-Si and Si-Mo-Si angles; the thickness layer (t); the cohesive energy per atom, (E_{coh}); the charge transfer (ΔQ) between atoms; the work function (Φ); the band gap (E_g) within PBE functional; and VBM/CBM positions, respectively.

	a,b (Å)	$d_{1,2}$ (Å)	d_3 (Å)	$\theta_{1,2}$ (°)	$\theta_{3,4}$ (°)	t (Å)	E_{coh} (eV/atom)	$\Delta Q_{1,2}$ (e)	Φ (eV)	E_g (eV)	VBM/CBM
MSN-1L	2.91	1.75,1.74	2.09	112,106	73,87	7.01	-8.46	2.99,1.5	5.12	1.79	Γ/K
MSN-2L	2.92	1.73,1.75	2.07	113,105	72,83	7.04	-7.46	2.20,1.5	5.10	1.60	Γ/K

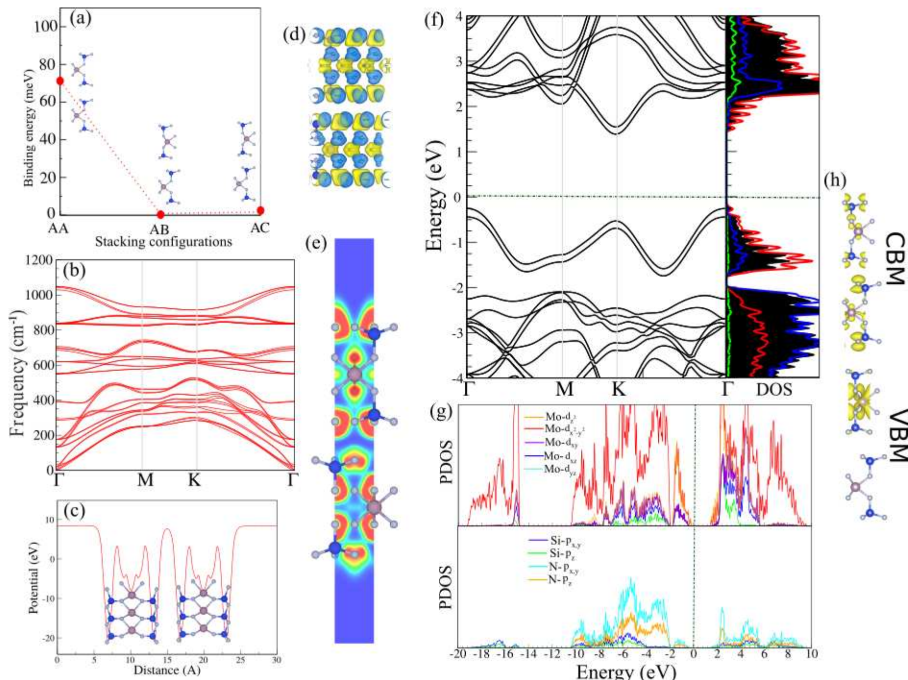

Figure 2. (a) Atomic structure, (b) phonon band dispersion, (c) contour plot of the electron localization function (ELF), (d) electronic band structure and (e) DOS and PDOS of the MSN-2L. The primitive unit cell is indicated by a red hexagonal. Charge densities of the valance band maximum (VBM) and conduction band minimum (CBM) states are shown in the inset of (e). The zero of energy is set to the Fermi-level.

states (DOS), and partial DOS (PDOS) of MSN-1L is exhibited in Fig. 1(d) and 1(e), respectively. Our results demonstrate that MSN-1L is an indirect semiconductor with a band gap of 1.79 eV. These results are in good agreement with a previous report.[35] The valence band maximum (VBM) and conduction band minimum (CBM) are located at the Γ and the K-point, respectively, indicated by the green point in Fig. 1(e). The VBM mainly originates from Mo-d_{z^2} and Mo-$d_{x^2-y^2}$ states, with a minor contribution of Si-p_z and N-p_z states, representing σ(Mo-Mo) bonding hybridized with σ(N-Si) bonding (see Fig. 1(e)). The CBM is solely composed of Mo-d_{z^2} states, representing σ(Mo-Mo) bonding.

IV. BILAYER

By stacking two layers of MSN-1L vertically, we consider several stacking geometries, i.e. AA, AB and AC (see Fig. 2(a)). We find that the minimum energy configuration is the AB-stacking arrangement. The binding of MSN-2L is plotted as a function of interlayer distance, as shown in Fig. S1(c). The minimum energy shows that the equilibrium distance is 3.21 Å, which is typical of interlayer spacing in van der Waal's bonded layered systems. The MSN-2L has a binding energy of -121 meV which means that the formation of the bilayer structure is exothermic and has a thermodynamic stability. The calculated bond lengths of C-C and C-N are 2.58 Å and 2.59 Å, respectively, while the bond angles are 119°. The electronic band structures and DOS/PDOS of MSN-2L are depicted in Fig. 2(d). The MSN-2L structure is a semiconductor with an indirect band gap of 1.60 eV (PBE) and 1.80 eV (HSE06). The VBM of MSN-2L is located at the Γ point, while the CBM is located at the K-point which are similar to MSN-1L. From the DOS/PDOS, we can see that the VBM mainly originates from Mo-d_{z^2} and Mo-$d_{x^2-y^2}$ states, while there is a minor contribution of

the Si and N p-states (see Fig. 2(d)).

V. ELECTRIC FIELD EFFECT

The presence of the interlayer distance in MSN-2L leads to a potential difference between the two atomic layers, which is very useful in tuning the electronic properties. In the following, the effect of an applied E-field on the electronic properties of MSN-2L is investigated. Tuning of the band gap is highly desirable for potential device applications and can be achieved by e.g. controlling the Fermi-level via application of an E-field. The electronic band structures of MSN-2L as a function of a perpendicular E-field in the parallel and antiparallel directions, perpendicular to the surface, are illustrated in Fig. 3(a) and 3(b), respectively. E-field >0 and <0 denote parallel and antiparallel to the z-axis. We find that the electronic structure is strongly modified by the application of an E-field. In the absence of E-field (0 V/Å), the band gap of MSN-2L is 1.6 eV (PBE). On applying a

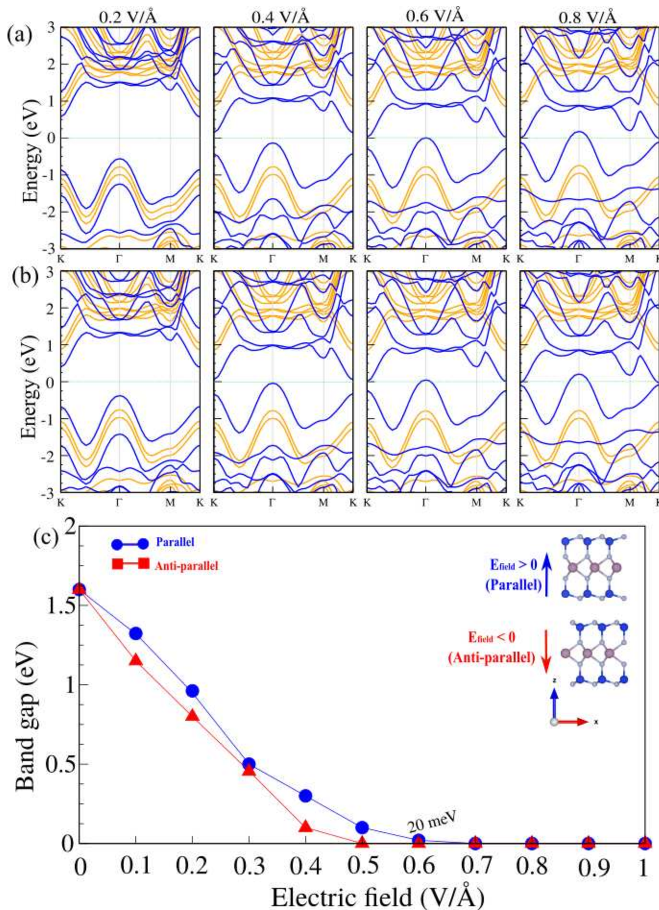

Figure 3. Electronic band structure of MSN-2L for (a) parallel and (b) antiparallel E-fields. The E-field strength varies from 0.1 to 1 V/Å. (c) Band gap of MSN-2L as a function of the E-field. The atomic structure and applied E-fields are shown in the inset. The zero of energy is set to the Fermi-level.

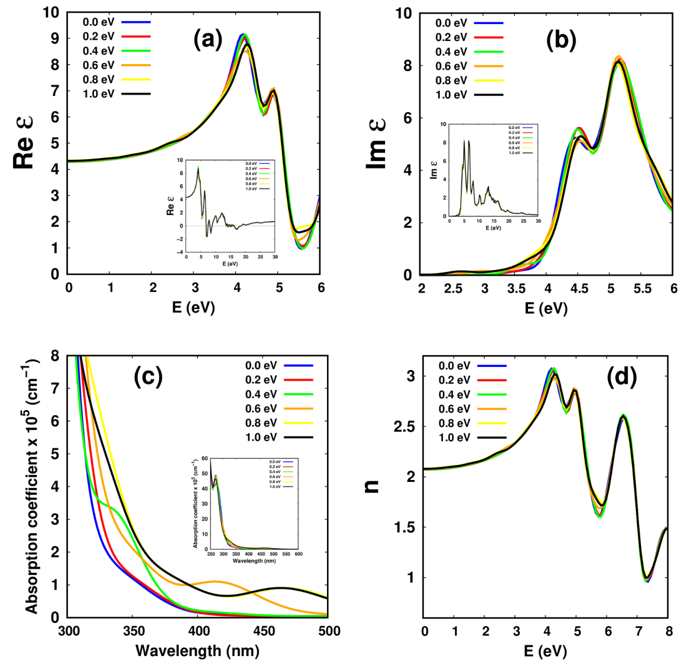

Figure 4. (a) Real and (b) imaginary parts of the dielectric constant. (c) Absorption coefficient (d) refractive index of the MSN-2L for different applied E-fields.

parallel E-field, the band gap decreases to 1.35, 1.15, 0.5, 0.3 and 0.1 eV for strengths 0.1-0.5 V/Å. With further increase of the E-field to 0.6 V/Å, there is a narrow band gap of ∼20 meV (see Fig. 2(c)). For an E-field strength of 0.6 V/Å, a semiconductor-to-metal transition occurs, and for an E-field from 0.6 to 1 V/Å, the metallic character is preserved. The electronic structure of MSN-2L for application of E-fields anti-parallel is similar to that in the parallel direction (Fig. 3(b)). The negative E-field decreases the band gap to 1.2 eV (0.1 V/Å), 0.8 eV (0.2 V/Å), 0.45 eV (at 0.3 V/Å). The band gap reaches 0.1 eV at 0.4 V/Å and for further increase of the E-field to 1 V/Åa semiconductor to metal electronic transition occurs at the E-field of 0.5 V/Å. For the E-field varying from 0.6 to 1 V/Å, the metallic character remains. The band gap as a function of the E-field in both directions is depicted in Fig. 3(c).

To gain insight into the optical response of the considered material, we simulate the effect of applying an external electrical field on its optical properties. One of the most important optical parameters of a material is the complex dielectric function. From the complex dielectric function, the optical properties, such as absorption and the reflectivity coefficient, can be calculated. Figure 4(a) shows the real part of the dielectric constant at different applied E-fields. Notably, in the energy range of 0 eV to 3.6 eV, the real part of the dielectric function is not majorly altered by increasing the applied E-field; the major changes in the real part of the dielectric constant appear in the peaks around 4.0 eV, 4.8 eV and 5.5 eV. However, for the higher energy region, as the field increases, a small

shift of the peak at 4.0 eV is observed and also the effects of the applied field on the optical properties can be seen more in the UV region. The inset indicates the spectrum of the real part of the dielectric constant over a wide energy range for various values of E-field. Fig. 4(b) shows the imaginary part of the dielectric constant. As can be seen from Fig. 4(b), as the field increases, a small change in the spectrum is observed, not only in the visible light region but also in the UV region of the electromagnetic spectrum. In the inset, the imaginary part of the dielectric constant at different applied fields for a wide range of energy is exhibited.

Finally, Figs. 4(c) and (d) demonstrate the evolution of the absorption and refractive index for different applied external fields. It can be seen that as the E-field increases, the absorption coefficient of the material increases in the visible light region (see Fig. 4(c)). Moreover, the inset figure reveals that the absorption spectrum also experiences a considerable change in the UV region as clearly seen for the energy of around 275 nm. Furthermore, based on our calculations, as seen in Fig. 4(d), the refractive index of the bilayer is insignificantly affected by applied external field, as only a very small change in the ultraviolet spectrum at 4.4, 4.8, 5.8, and 7.2 occurs on increasing the E-field.

The behavior of the monotonically decreasing bandgap with increasing the vertical field is similar to 2D hexagonal boron nitride (BN),[55] MoX_2 (X=S, Se, Te) and WX_2 (X=S and Se) bilayers.[57] The electric field decreases the fundamental band gap of the BN bilayer and at large fields (more than 0.6 V/Å, critical field) a complete semiconductor-metal transition appears. The MoX_2 and WX_2 are semiconductors with bandgaps of 1-1.5 eV.[53,54] The increase in the vertical electric fields to these bilayers decreases their bandgaps. Furthermore, the large external field (critical field) can induce the semiconductor-metal transition in the range of 0.20.3 V/Å which is smaller than the critical applied field to get the corresponding transition in the hexagonal boron nitride bilayer.[57] The critical field depends on the fundamental bandgap of the bilayer, as the fundamental bandgap increases the critical field increases. In addition for many MoX_2/WX_2 heterostructures, the decreasing of the bandgap with increasing the applied field is noticed.[43] For graphene bilayer, the normal applied external electric field breaks the inversion symmetry of the bilayer structure and opens a bandgap that is continuously tunable up to about 250 meV.[56]

VI. STRAIN EFFECT

It is well known that by applying external vertical strain the performance of a layered material for use in device applications can be effectively improved. For the case of 2D graphene-based heterostructures, it has been confirmed that the tailoring of interlayer spacing, which can be experimentally controlled by nano-mechanical pressure,[36] is an effective approach to modulate the electronic properties of the materials. Many experiments of the in-plane mechanical properties of 2D structures are established.[51,52] The experimental investigations of the out-of-plane (vertical) mechanical properties are still have some technical difficulties due to the small interlayer distance.[45] The out-of-plane properties can be explored directly by applying normal force to 2D structures using unconventional AFM-based method[46] and friction force microscopy (FFM)[47,48] or indirectly by Raman spectroscopy.[49,50] The mono-, bi- and few-layers of graphene have experimentally studied in more detail.[63,67] It is found that the addition of an ethanol/methanol mixture or helium can increase this distance between the layers[63] which means we can control the vertical (out-of-plane) strain using this technique. The distance between the layers can be measured by Lynch and Drickamer.[66] Furthermore, the relative rotation angle (0° to 10°) between the two layers (heterostructures) can change the out-of-plane strain which agrees with experimental results.[59] At large in-plane strain variation on MoS_2/WSe_2 heterobilayer, it is found the out-of-plane displacement strain greatly improves the agreement between theoretical and the experimental results.[60] The applying out-of-plane strains, can effectively control the electronic properties of graphene-based vdW heterostructures and be carried out in the experiment by nanomechanical pressure,[61] vacuum thermal annealing[63] and so on.[64,65]

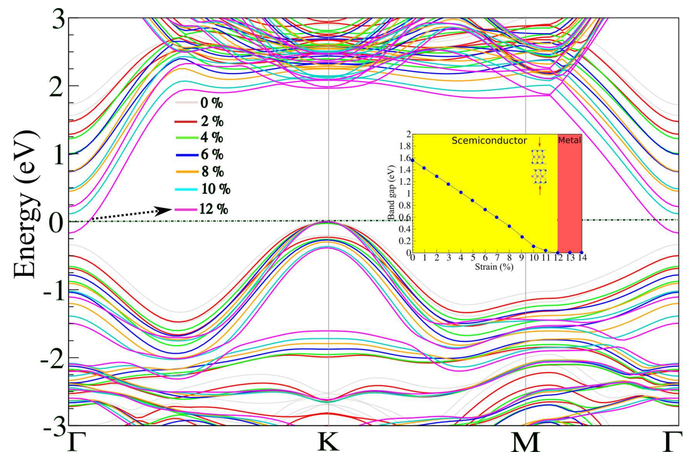

Figure 5. Electronic band structure of the MSN-2L for application of vertical compressive strain. The zero of energy is at the Fermi-level.

Regarding theoretical investigations, the effect of vertical strain on the electronic structures of bilayer, heterostuctres, heterojunctions 2D materials has been studied.[43,44] Here, we further analyzed the effects of applying an external vertical compressive strain on the electronic and optical characteristics of the MSN-2L. In these calculations, the strain coefficient (ε) is defined as, $\varepsilon = (d - d_0)/d_0 \times 100$ in which d_0 and d are the interlayer distance for unstrained and strained bilayers, respectively

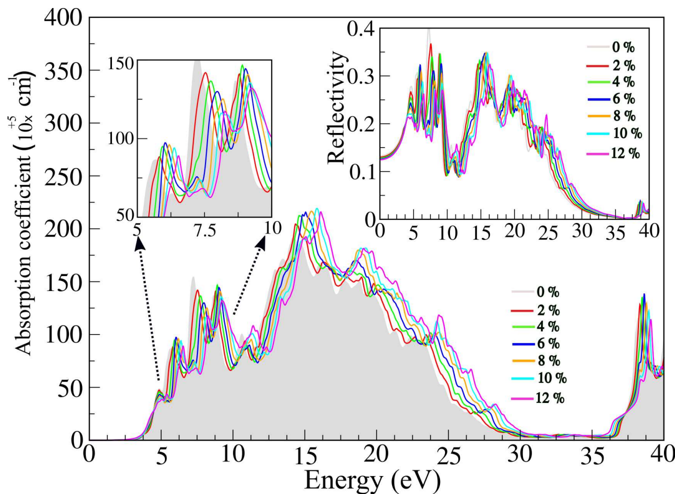

Figure 6. Optical absorption spectral dependencies of the strained MSN-2L. Reflectivity characteristics indicated as inset.

and we consider ε=2-12%. Fig. 5 illustrates the calculated electronic band structure of MSN-2L under external vertical compressive strain. As the compressive vertical strain increases, the band gap of the bilayer linearly decreases while it remains an indirect semiconductor. Moreover, one can see that a semiconductor-metal phase transition occurs at about 12% strain. The decreasing bandgap under normal compressive strain is found in the $PtSe_2$ bilayer[58] and MoX_2/WX_2 heterostructures.[43] Furthermore, it can be observed that by increasing the vertical strain, the charge carrier mobility is slightly increased as the effective mass of the charge carriers is slightly reduced; the curvature of the band is proportional to the charge carrier mobility of the material.

To shed light on the effect that the application of an external vertical strain has the optical properties, we demonstrate in Fig. 6 the optical absorption and reflectivity properties for perpendicular polarization E∥z. As can be seen that the structure shows considerable absorption and reflectivity in the UV region of the electromagnetic spectrum, where the many absorption peaks within the considered energy range are related to the inter-band transitions. Also, it can be seen that by applying vertical compressive strain, both the positions and intensities of the absorption and reflectivity peaks are slightly decreased, while the absorption edge exhibits a strong blue-shift for ε=0 to ε=12%. The obtained results suggest MSN-2L is an interesting candidate for use in electro-mechanical sensing devices as well as in UV light shielding and sensing applications.

VII. CONCLUSION

We have investigated the structures, electronic, and optical properties of the $MoSi_2N_4$ monolayer (MSN-1L) and bilayer (MSN-2L), including the impact of an applied E-field and strain, by means of first-principles calculations. For MSN-2L, the electronic properties can be strongly modified by an E-field and strain. When the E-field increases from 0.1 to 0.6V/Å, the band gap decreases linearly. Interestingly, for the parallel E-field > 0.5V/Å and antiparallel E-field > 0.4V/Å, a narrow band gap develops with values of 20 meV and 0.10 meV, respectively. For E-field >0.6, the semiconductor character of MSN-2L becomes a metal for both E-field directions. Depending on the direction of the applied E-field, the band gap of MSN-2L is modified to slightly different values. The effect of compressive, out-of-plane (vertical) strain, on the electronic properties of MSN-2L demonstrates that they can be efficiently engineered by applying external strain. Notably, we find that a vertical compressive strain decreases the band gap of the MSN-2L and a semiconductor to metal transition occurs for a vertical compressive strain of about 12%. The transition is a result of opposite energy shifts of states in the two layers. Analyzing the optical properties, we find a strain tunable optical response for the MSN-2L structure in the *UV* region of the electromagnetic spectrum. These strain tunable electronic and optical properties are very promising in terms of novel nano-devices designing. Therefore, we expect that our theoretical study will stimulate further experimental research on MSN-2L. It might be a candidate material for the realization of technological applications requiring electrically tunable band gaps such as future electro-mechanical and opto-mechanical devices.

VIII. CONFLICTS OF INTEREST

The authors declare that there are no conflicts of interest regarding the publication of this paper.

IX. SUPPLEMENTARY MATERIAL

See supplementary material for the computational details for optical properties calculations.

X. ACKNOWLEDGMENTS

This work was supported by the National Research Foundation of Korea (NRF) grant funded by the Korea government (MSIT) (NRF-2015M2B2A4033123).

XI. DATA AVAILABILITY STATEMENT

The data that support the findings of this study are available from the corresponding author upon reasonable request.

* bafekry.asad@gmail.com

1 K. S. Novoselov, A. K. Geim, S. V. Morozov, D. Jiang, Y. Zhang, S. V. Dubonos, I. V. Grigorieva, A. A. Firsov, Sci., 306, 5696, (2004) 666-669.

2 M. T. Hwang, M. Heiranian, Y. Kim, S. You, J. Leem, A. Taqieddin, V. Faramarzi, Y. Jing, I. Park, A. M. van der Zande, S. Nam, N. R. Aluru, R. Bashir, Nat. Commun. 11, (2020),1543.

3 B. Mortazavi, A. Bafekry, M. Shahrokhi, T. Rabczuk, X. Zhuang, Materials Today Energy, 16, (2020), 100392.

4 L. Xue, S. Li, T. Shen, M. Ni, C. Qiu, S. Sun, H. Geng, X. Zhu, H. Xia, Energy Storage Mater., 32, (2020), 272-280.

5 M. K. Mohanta and A. De Sarkar, ACS Appl. Mater. Inter., 12, 2020, (15), 18123-18137.

6 R. Wang, Z. Li, S. Li, P. Wang, J. Xiu, G. Wei, H. Liu, N. Jiang, Y. Liu, and M. Zhong, ACS Applied Materials and Interfaces, 12, 37, (2020), 41919-41931.

7 Z. Wang, T. Yang, Y. Zhang, Q. Ou, H. Lin, Q. Zhang, H. Chen, H. Y. Hoh, B. Jia, Q. Bao, Adv. Mater. 32, (2020), 20001388.

8 S. Parveen, K. K. Paul, and P. K. Giri, ACS Appl. Mater. Inter., 12, 5, (2020), 6283-6297.

9 A. K. Geim, Sci., 324, 5934, (2009), 1530-1534.

10 J. Xu, X. Hu, X. Wang, X. Wang, Y. Ju, S. Ge, X. Lu, J. Ding, N. Yuan, Y. Gogotsi, Energy Storage Materials, 33, (2020), 382-389.

11 A. Bafekry, C. V. Nguyen, C. Stampfl, B. Akgenc, and M. Ghergherehchi, Phys. Status Solidi B. (2020).

12 A. Bafekry, B. Akgenc, M. Ghergherehchi and F. M. Peetersm J. Phys.: Condens. Matter, 32, (2020), 355504.

13 A. Bafekry, M. Yagmurcukardes, B. Akgenc, M. Ghergherehchi, and Ch. V. Nguyen, J. Phys. D: Appl. Phys. 53, (2020), 355106.

14 Li. H. Li, and Y. Chen, Adv. Funct. Mater, 26, (2016), 2594-2608.

15 A. Bafekry, Physica E: Low-dimensional Systems and Nanostructures, 118, (2020), 113850.

16 A. Bafekry, C. Nguyen, M. M. Obeid and M. Ghergherehchi, New J. Chem., 44, (2020), 15785-15792.

17 A. Bafekry, C. V. Nguyen, A. Goudarzi, M. Ghergherehchi and M. Shafieirad, RSC Adv., 10, (2020) 27743-27751.

18 M. M. Obeid, C. Stampfl, A. Bafekry, Z. Guan, H. R. Jappor, C. V. Nguyen, M. Naseri, D. M. Hoat, N. N. Hieu, A. E. Krauklis, V. Vu, Tuan D. Gogova, Phys. Chem. Chem. Phys, 22, 27, (2020), 15354-15364.

19 A. Bafekry, M. Ghergherehchi and S. Farjami Shayesteh, Phys. Chem. Chem. Phys., 21, (2019),10552-10566.

20 A. Bafekry, S. Farjami Shayesteh and F. M. Peeters, Phys. Chem. Chem. Phys., 21, (2019), 21070-21083.

21 A. Bafekry, and M. Neek-Amal, Phys. Rev. B, 101, 8, (2020), 085417.

22 H. T. T. Nguyen, M. M. Obeid, A. Bafekry, M. Idrees, V. V. Tuan, V. H. Phuc, N. H. Nguyen T. L. Hoa, B. Amin, Bin and V. C. Nguyen, Phys. Rev. B, 102, 7, (2020), 075414.

23 A. Bafekry, C. Stampfl, M. Ghergherehchi, Nanotechnol., 31, (2020), 295202.

24 A. Bafekry, C. Stampfl, and F.M. Peeters, Phys. Status Solidi B, 257, (2020), 2000182.

25 A. Bafekry, C. Stampfl, F. M. Peeters, Sci. Rep. 10, 213 (2020).

26 A. Bafekry, S. Farjami Shayesteh, and F. M. Peeters, J. Appl. Phys., 126, 21, (2019), 215104.

27 A. Bafekry, S. Farjami Shayesteh, M. Ghergherehchi, and F. M. Peeters, J. Appl. Phys., 126, 14, (2019), 144304.

28 A. Bafekry, B. Mortazavi, S. Farjami Shayesteh, J. Magnetism and Magnetic Materials, 491, (2019), 165565.

29 A. Bafekry, M. Yagmurcukardes, M. Shahrokhi, M. Ghergherehchi, Carbon, 168, (2020), 220-229.

30 A. Bafekry, Physica E: Low-dimensional Systems and Nanostructures, 118, (2020), 113850.

31 A. Bafekry, C. Stampfl, M. Ghergherehchi, S. Farjami Shayesteh, Carbon, 157, (2020), 371-384.

32 Y. Lan, L. X. Xia, T. Huang, W. Xu, G. F. Huang, W. Hu and W. Q. Huang, Nanoscale Research Letters, 15, (2020), 180.

33 M. Luo and H. Yin, Integrated Ferroelectrics, 211, 1, (2020), 167-174.

34 A. Bafekry, M. Faraji, D.M. Hoat, M. Shahrokhi, M. M. Fadlallah, F. Shojaei, S. A. H. Feghhi, M. Ghergherehchi, D. Gogova, J. Phys. D: Appl. Phys., 54, 15, (2021), 155303.

35 Y. L. Hong, Z. Liu, L. Wang, T. Zhou, W. Ma, C. Xu, S. Feng, L. Chen, M. L. Chen, D. M. Sun, X. Q. Chen, H. M. Cheng, W. Ren, Sci., 369, 6504, (2020), 670-674.

36 H.V. Phuc, N.N. Hieu, B.D. Hoi, C.V. Nguyen, Phys. Chem. Chem. Phys., 20 (2018), 17899.

37 P. Blaha, K. Schwarz, G. Madsen, D. Kvasnicka, J. Luitz and K. Schwarz, Techn. Universitat. (2019).

38 J. P. Perdew, K. Burke, and M. Ernzerhof, Phys. Rev. Lett. **77**, 3865 (1996).

39 J. P. Perdew, K. Burke, and M. Ernzerhof, Phys. Rev. Lett. **78**, 1396 (1997).

40 G. Henkelman, A. Arnaldsson, and H. Jonsson, Comput. Mater. Sci. **36**, 354 (2006).

41 H.J. Monkhorst and J.D. Pack, Phys. Rev. B **13**, 12, (1976).

42 D. Alfe, Comput. Phys. Commun. **180**, 2622 (2009).

43 Sharma, Munish and Kumar, Ashok and Ahluwalia, P. K. and Pandey, Ravindra, Journal of Applied Physics, **116**, 063711 (2014).

44 Bafekry, Asadollah and Gogova, Daniela and M. Fadlallah, Mohamed and V. Chuong, Nguyen and Ghergherehchi, Mitra and Faraji, Mehrdad and Feghhi, Seyed Amir Hossein and Oskoeian, Mohamad, Phys. Chem. Chem. Phys. **23**, 4865 (2021).

45 Oviedo, Juan Pablo and Kc, Santosh and Lu, Ning and Wang, Jinguo and Cho, Kyeongjae and Wallace, Robert and Kim, Moon, ACS nano **9**, 1543 (2014).

46 Gao, Yang and Kim, Suenne and Zhou, Si and Chiu, Hsiang-Chih and Nelias, Daniel and Berger, Claire and Heer, Walt and Polloni, Laura and Sordan, Roman and Bongiorno, Angelo and Riedo, Elisa, Nature materials **14**, 714 (2015).

47 Liu, Ze and Yang, Jiarui and Grey, Francois and Liu, Jefferson Zhe and Liu, Yilun and Wang, Yibing and Yang, Yanlian and Cheng, Yao and Zheng, Quanshui, Phys. Rev. Lett. **108**, 205503 (2012).

48 Zheng, Quanshui and Jiang, Bo and Liu, Shoupeng and Weng, Yuxiang and Lu, Li and Xue, Qikun and Zhu, Jing and Jiang, Qing and Wang, Senhu and Peng, Lian-Mao, Phys. Rev. Lett. **100**, 067205 (2008).

[49] Cong, C. and Yu, Ting, Nature communications **5**, 4709 (2014).
[50] Mikai Chen and Hongsuk Nam and H. Rokni and Sungjin Wi and Jeong Seop Yoon and Peng-Yu Chen and K. Kurabayashi and W. Lu and X. Liang, ACS nano **9**, 8773 (2015).
[51] Koenig, Steven and Boddeti, Narasimha and Dunn, Martin and Bunch, Joseph, Nature nanotechnology **6**, 543 (2011).
[52] Bunch, Joseph and Verbridge, Scott and Alden, Jonathan and Zande, Arend and Parpia, Jeevak and Craighead, Harold and Mceuen, Paul, Nano letters **8**, 2458 (2008).
[53] Böker, Th. and Severin, R. and Müller, A. and Janowitz, C. and Manzke, R. and Voß, D. and Krüger, P. and Mazur, A. and Pollmann, J., Phys. Rev. B **64**, 235305 (2001).
[54] Klein, A. and Tiefenbacher, S. and Eyert, V. and Pettenkofer, C. and Jaegermann, W., Phys. Rev. B **64**, 205416 (2001).
[55] Yang, Zailin and Ni, Jun, J. App. Phys. **107**, 104301 (2010).
[56] Zhang, Yuanbo and Tang, Tsung-Ta and Girit, Caglar and Hao, Zhao and Martin, Michael and Zettl, Alex and Crommie, Michael and Shen, Y and Wang, Feng, Nature **459**, 820 (2009).
[57] Ramasubramaniam, Ashwin and Naveh, Doron and Towe, Elias, Phys. Rev. B **84**, 205325, (205325).
[58] Li, Pengfei and Li, Lei and Zeng, Xiao Cheng, J. Mater. Chem. C **4**, 3106 (2016).
[59] Kumar, Hemant and Er, Dequan and Dong, Liang and Li, Junwen and Shenoy, Vivek, Scientific reports **5**, 10872 (2015).
[60] Waters, Dacen and Nie, Yifan and Lupke, Felix and Pan, Yi and Folsch, Stefan and Lin, Yu-Chuan and Jariwala, Bhakti and Zhang, Kehao and Wang, Chong and Lv, Hongyan and Cho, Kyeongjae and Xiao, Di and Robinson, Joshua and Feenstra, R., ACS Nano **14**, 7564 (2020).
[61] M. Dienwiebel, G. S. Verhoeven, N. Pradeep, J. W. M. Frenken, J. A. Heimberg and H. W. Zandbergen, Phys. Rev. Lett. **92**, 126101 (2004).
[62] S. Tongay , W. Fan , J. Kang , J. Park , U. Koldemir , J. Suh , D. S. Narang , K. Liu , J. Ji and J. Li, Nano Lett. **14**, 3185 (2014).
[63] S. M. Clark , K. J. Jeon , J. Y. Chen and C. S. Yoo , Solid State Commun. **154**, 15 (2013).
[64] H. Fang, C. Battaglia, C. Carraro, S. Nemsak, B. Ozdol, J. S. Kang, H. A. Bechtel , S. B. Desai, F. Kronast and A. A. Unal, Proc. Natl. Acad. Sci. U. S. A. **111**, 6198 (2014).
[65] G. Giovannetti , P. A. Khomyakov , G. Brocks , P. J. Kelly and J. V. D. Brink , Phys. Rev. B: Condens. Matter Mater. Phys. **76**, 3009 (2007).
[66] R.W. Lynch, H.G. Drickamer, J. Chem. Phys. **44**, 181 (1966).
[67] Proctor, John E. and Gregoryanz, Eugene and Novoselov, Konstantin S. and Lotya, Mustafa and Coleman, Jonathan N. and Halsall, Matthew P., Phys. Rev. B **80**, 073408 (2009).

View publication stats